Taking Average-Power, Diode-Pumped, Solid-State Lasers beyond the Nd^{3+} Ion

R. J. Beach

C. Bibeau

E. C. Honea

S. B. Sutton

Introduction

Diode lasers have long been strategically viewed as the ultimate replacement for flashlamp and arc lamp radiation sources used to pump solid-state lasers. Diode semiconductor lasers, first demonstrated in 1963, directly convert electric current into laser photons at a semiconductor junction.[1] Today, such lasers exhibit electrical-to-optical conversion efficiencies in excess of 50% (Ref. 2). By varying the composition of semiconductor materials during growth of the laser diode crystal, emission wavelength can be tuned over a broad range that covers many rare-earth-ion absorption features. The properties of high efficiency and flexible wavelength generation, along with dramatic improvements in performance and device reliability over the last several years, make laser diode arrays viable pump excitation sources for solid-state lasers using rare-earth-ion-doped crystalline gain materials.

The impact of semiconductor lasers on the development of solid-state lasers is most evident in the high-average-power, solid-state laser systems that are finding wide application in the field of materials processing. High-average-power, diode-pumped, solid-state lasers (commonly referred to as HAP DPSSLs) are best characterized as being performance-limited by thermal management issues associated with the solid-state laser crystal or glass. Thermal management issues can manifest themselves in several different forms, such as optical quality aberration of the output laser beam due to thermally induced optical refractive index variations in the crystal and, in extreme cases, fracture of the laser crystal due to buildup of excessive stress in the crystal.

The most common ion/host crystal combination used in HAP DPSSL systems today is Nd^{3+}:YAG (Ref. 3). Of all the well developed laser crystals that can be grown with rare-earth impurities, YAG (yttrium-aluminum-garnet) is the most robust in a thermal sense—i.e., it has the highest thermal conductivity and resistance to fracture. Thus, YAG is the crystalline host of choice for HAP DPSSLs. The wide use of Nd^{3+} as the active ion in nearly all HAP DPSSLs is associated with several fortuitous coincidences between the pump irradiance and wavelength required to efficiently excite it, and the pump irradiance and wavelength that can be conveniently developed by AlGaAs semiconductor 2D laser diode arrays. AlGaAs is the most mature of the semiconductor laser materials in use today.

Although the Nd^{3+} ion now dominates the HAP DPSSL field, the situation could change in the future because of continued technical developments in laser diode arrays. One such development, which has been actively pursued by the Lawrence Livermore National Laboratory's Laser Programs, is a diode array pump technology that enables pump power to be delivered at much higher irradiances than was previously possible.[4] Because many rare-earth-ion-based HAP DPSSLs are only practical if pumped at higher irradiances than the several kW/cm^2 possible with conventional scaled diode array technologies, this approach has opened a path to HAP DPSSLs that rely on ions other than Nd^{3+} as the lasant. We have demonstrated several such systems by taking advantage of the new flexibility in active lasant ion. Two of the systems, which lead the world for average power generation in their respective class, are our HAP Tm:YAG and Yb:YAG DPSSLs, which generate output radiation at 2 and 1 μm, respectively. These two laser systems, along with our end-pumping technology, are the focus of this article.

Scalable Diode End Pumping

The stumbling block in developing a scalable diode end-pumping architecture has been the intrinsically low effective radiance of the 2D emitting apertures constructed from a stack of laser diode array bars. Figure 1 shows the packaging technology developed within the Laser Programs, which uses a silicon, microchannel-cooled, diode-bar heatsink, and is designed to be stacked to build up large emitting apertures.[5] The low effective radiance of arrays results from the fact that the diode radiation is generated in a waveguide structure having at least one transverse dimension approximately equal to the radiation wavelength. The result is a beam of radiation with high divergence angle, up to 60° in one dimension, commonly referred to as the fast axis direction.

The key to overcoming low radiance in the fast axis direction of diode arrays is optical conditioning of the diode radiation from individual bars. A very-high-precision cylindrical microlens developed in our group does just that. The microlens can be produced in quantity at very low cost using a shaped-fiber-pulling technique.[6] Figure 2(a) is a cross-sectional view of one of our Si microchannel-cooled packages with a microlens in place.[7] The radiation, diverging at

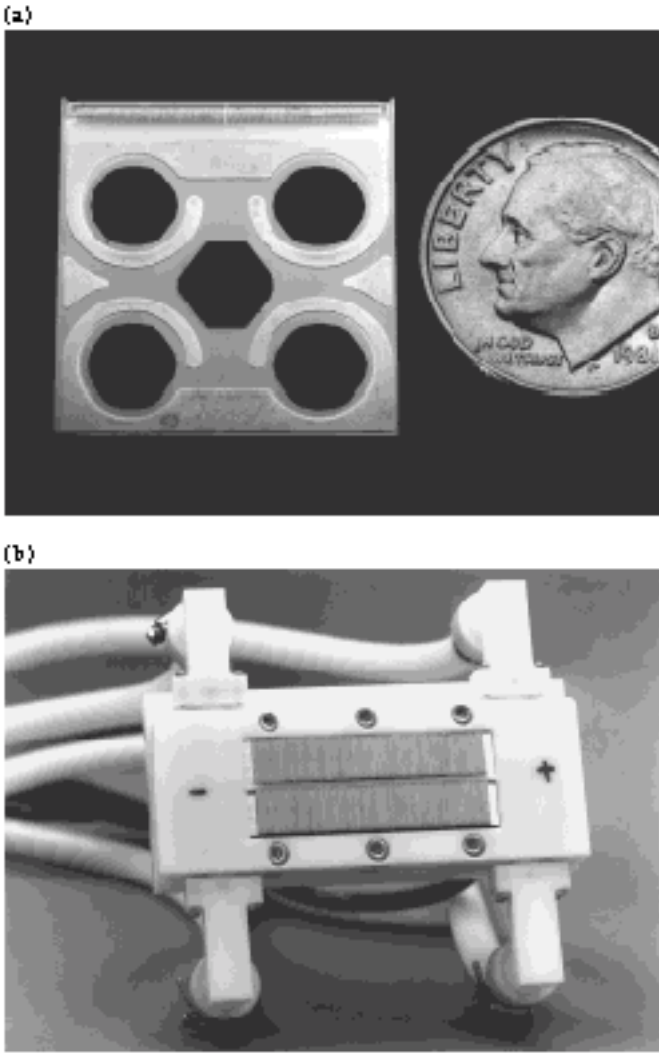

FIGURE 1. (a) Si, microchannel-cooled, laser diode module developed at LLNL. Dime shown for size comparison. (b) 2D stack of Si, microchannel-cooled, laser diode modules developed at LLNL. (99-50-0693-2304pb01)

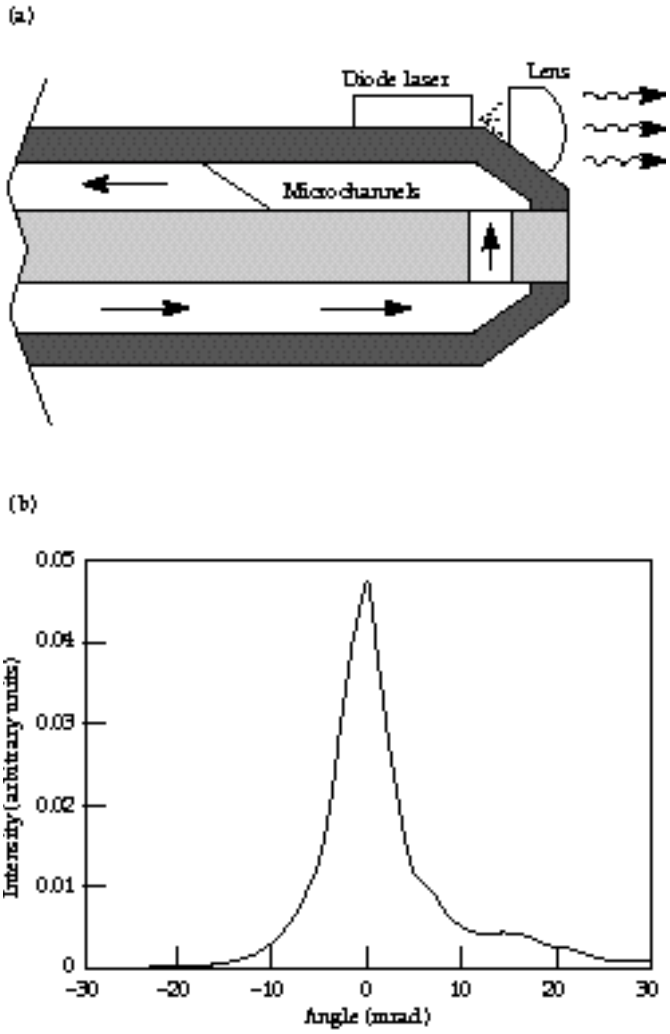

FIGURE 2. (a) Cross-sectional view of the LLNL silicon, microchannel-cooled, laser diode module with a cylindrical microlens. (b) Fast-axis, far-field intensity profile of a microlens conditioned package. (99-50-0595-1257pb02)

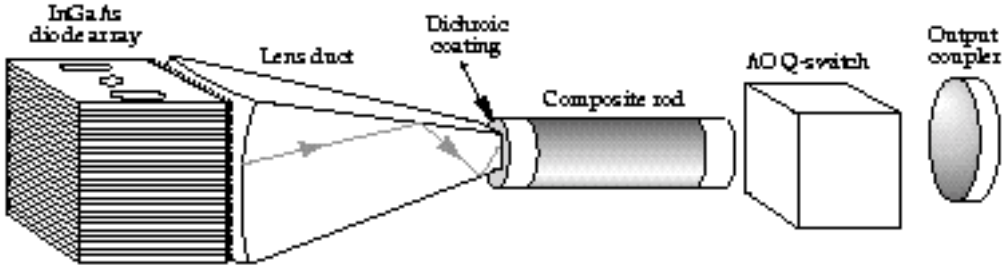

FIGURE 3. Schematic of a typical diode end-pumped and Q-switched laser. (99-50-0192-0153pb01)

approximately 60° out of the bar, is collected and collimated by the cylindrical microlens mounted on the front of the package. After collimation, divergence of the diode light is reduced to ~0.6° . Using such microlens packages to build up large arrays by stacking leads to overall fast-axis divergences that are reduced by a factor of ~100 compared to values without microlens conditioning. This decrease in divergence, together with the accompanying ability to focus radiation to a smaller spot than if no conditioning had been performed, enables the output of radiation from large, 2D diode stacks to be efficiently delivered to the end of rod lasers. Figure 2(b) is a plot of the variation in angular intensity of a typical laser diode package fitted with a cylindrical microlens.

Figure 3 shows a typical end-pumped laser system using our scalable end-pumping architecture. Pump radiation from the microlens-conditioned stack of laser diode packages is delivered to the laser rod by a device called a lens duct. This optical device delivers the pump radiation to the end of the laser rod with high efficiency and increased intensity. Lens ducts are fabricated from transparent optical materials. They rely on lensing at their curved input face and total internal reflection (TIR) at their canted planar faces to channel the diode pump radiation to the laser rod.[8]

The best way to visualize the operation of a lens duct is to consider a plane wave normally incident on a spherically curved input surface of an optical material, as shown in Figure 4. With the radius of curvature of the input face r and the index of refraction of the optical material n, the wave comes to a geometric focus at distance l into the material according to

$$l = r\frac{n}{n-1} \quad . \tag{1}$$

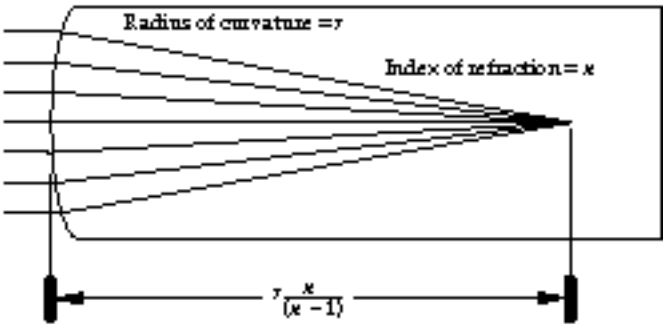

FIGURE 4. Focusing of a normally incident plane wave at a distance $rn/(n-1)$ into a material having an input radius of curvature r and index of refraction n. (99-50-0595-1258pb02)

For an extended incoherent source, such as a microlens-conditioned, 2D, semiconductor laser diode array, there is no single, well defined geometric focal spot. Rather, the transverse dimensions of the focal region are determined by the angular divergence of the radiation's source function. Unfortunately, with today's microlens-conditioned laser diode arrays, the focal region can easily overfill the aperture of a laser rod for many of the practical laser systems of interest to designers. However, by reshaping the object in Figure 4 to resemble the lens duct in Figure 3, it is possible to deliver most of the diode radiation to the end of a laser rod within the constraints imposed by Etendue invariance.[9] Using Figure 4 as a guide, it might be expected that the optimum design of a lens duct configured to couple diode radiation into a circular laser rod would be to adjust its length l from Eq. (1) and cant in its planar sides so that it has a square output end that just inscribes the circular end of the laser rod to be pumped. In this fashion, many of the rays that would be delivered outside of the rod aperture, without the canting in of the planar sides, could be efficiently channeled to the laser rod by making high-angle (near grazing incidence) TIRs off the planar sides of the lens duct. We find that length l from Eq. (1) is not optimal. Rather, the length should be somewhat shorter,

$$l_d = (0.92) r_d \frac{n_d}{n_d - 1} \quad . \tag{2}$$

The length shortening comes about because the minimum transverse dimension of the focal region occurs somewhat before the geometrical focus shown in Figure 3 and predicted by Eq. (1).

To better understand the optimization of lens ducts, we have developed a geometric "method-of-images" analysis that allows transfer efficiency studies to be performed quickly and easily.[8] When modeling the

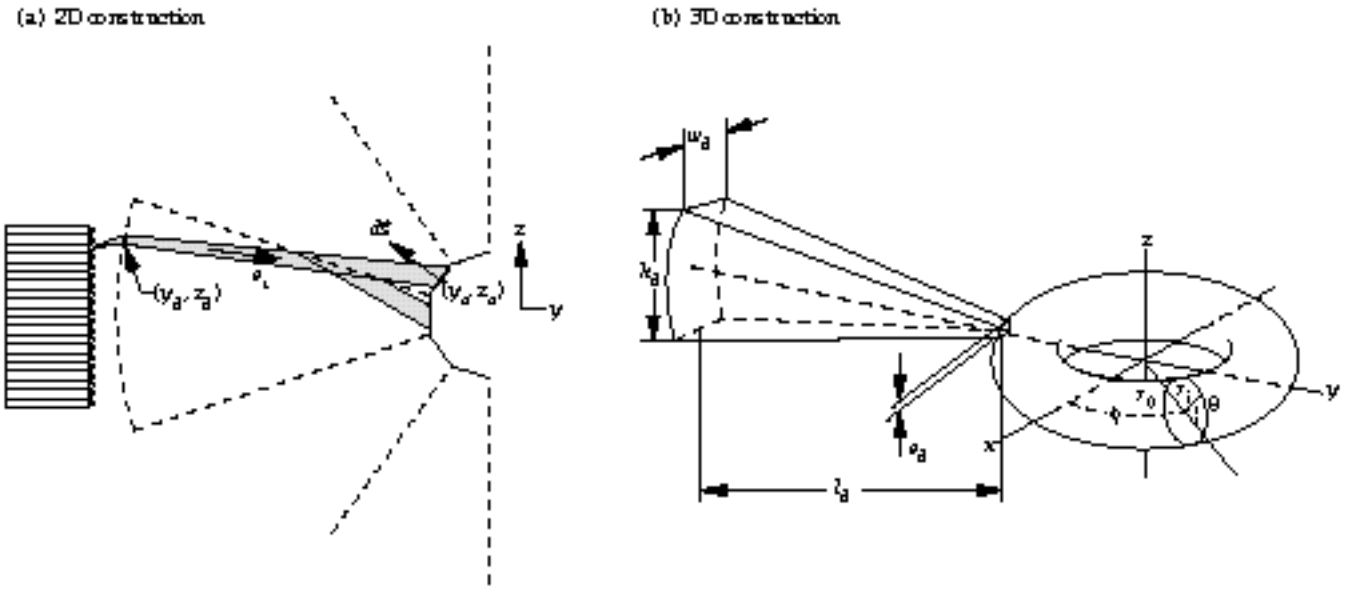

FIGURE 5. (a) 2D view of a lens duct showing the method-of-images construction used in calculating the transfer efficiency of radiation from a diode array into a laser rod. One bundle of rays bounces by total internal reflection off one of the canted planar sides of the lens duct; a related direct bundle of rays is also shown. (b) 3D lens duct and its method-of-images construction for a toroidal surface.
(99-50-0595-1259pb02)

transfer efficiency of lens ducts, the front input surface is straightforward to treat because it acts as a simple lens. However, complications arise in modeling the TIR bounces made by pump light off the canted planar sides of the duct. Nevertheless, the TIR bounces can be easily treated by using a simple trick.

Figure 5(a) shows a semicircular surface representing the lens duct output face and the rod pump input face. This illustration was generated using our method-of-images construction (here, we ignore the complication that the semicircular surface is actually faceted). This construction consists of repeatedly reflecting the lens duct about its TIR surfaces as shown. When tracing a particular bundle of rays from the diode array to the end of the lens duct, instead of reflecting the rays at their intersection with one of the canted planar duct sides, the rays can be traced straight through to their intersection with the generated semicircle. To calculate the transfer efficiency of the duct, it is only necessary to track those rays that leave the diode array and propagate along straight-line trajectories that intersect the semicircle. For any such bundle of rays, the transfer efficiency associated with the bundle is determined by reflective losses at the duct input and output surfaces. A complete calculation of transfer efficiency involves a double integral over two surfaces: the diode-array-emitting aperture, and the semicircle representing the output surface of the lens duct.

An extension from two to three dimensions is straightforward. Figure 5(b) shows the 3D method-of-images construction in which a toroidal surface is generated instead of a semicircle. The double integral used to calculate the transfer efficiency is now over the diode array aperture and that section of the 2D toroidal surface that faces the diode aperture. This technique to calculate transfer efficiencies allows quick optimization of lens duct structures and has been useful in defining rules of thumb for their design.

Although our method-of-images construction is an elegant and simple way to calculate transmission efficiencies of a lens duct, it has several practical limitations. The most serious is that the technique is only applicable to lens ducts with output ends that are either square or rectangular. Although these were the shapes in our early work, we have recently used ducts with output ends shaped like octagons. An octagon-shaped output end increases the area of the output end of the duct that must fit within the circular boundary defined by the rod end. An octagon inscribed within a circle has 40% more area than a square inscribed within the same circle. Because we are interested in coupling large diode array apertures into the ends of small rods, and we must respect Etendue invariance or the brightness theorem, the ability to use an octagon-shaped duct output with its larger area reduces the radiance requirements on the diode array.

Figure 6 shows a lens duct with an octagon-shaped output end that is being used in the diode-pumped NIF prototype regenerative amplifier heads.[10] To model these more advanced lens ducts, we have developed a Monte Carlo ray-tracing code that takes a brute-force approach and simply traces rays from the

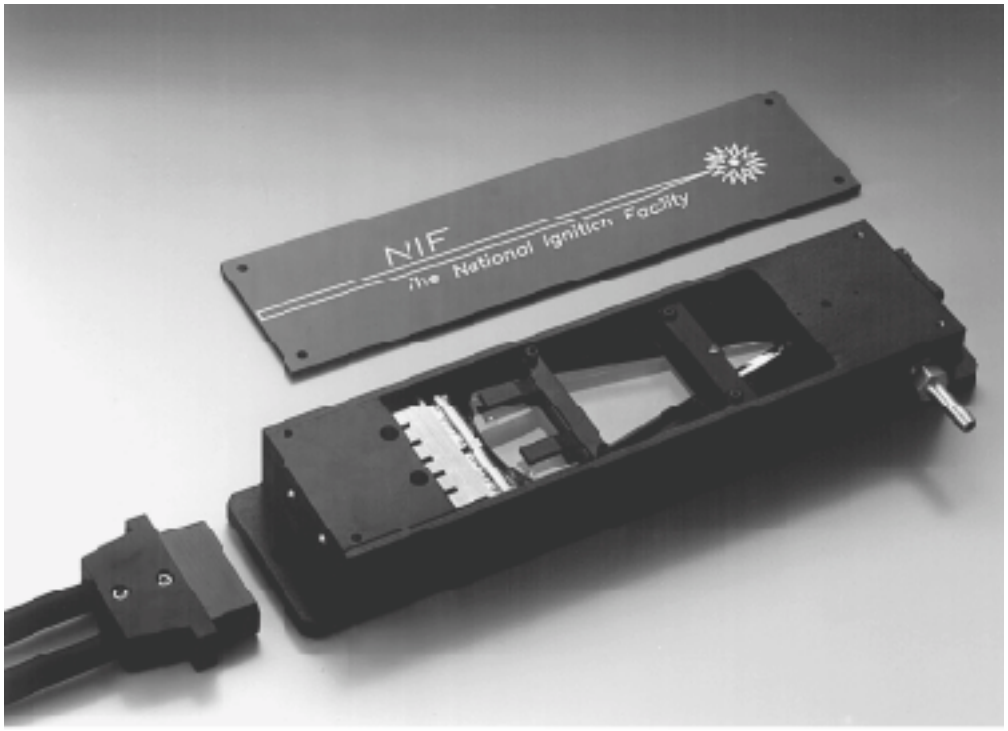

FIGURE 6. Photograph of a NIF regenerative amplifier head illustrating the compactness of a lens duct and laser diode array. (99-00-0595-1337pb02)

diode aperture through the system, including TIR bounces. Not only can we calculate transfer efficiencies with this code, but we can also calculate pump intensity profiles, both at the end of the lens duct and within the laser rod being pumped. Figure 7 shows the output from a code simulation run for the case of a lens duct used in our Yb:YAG system (discussed below). In addition to showing the pump light intensity profile at the end of the lens duct, this figure also shows the intensity profile at a selected cross-sectional plane within the laser rod, as well as the far-field intensity profile (or angular dependence) of the pump light that emerges from the duct.

After pump light emerges from the lens duct, it enters the laser rod through a dichroic optical coating designed to pass the pump light and act as a high

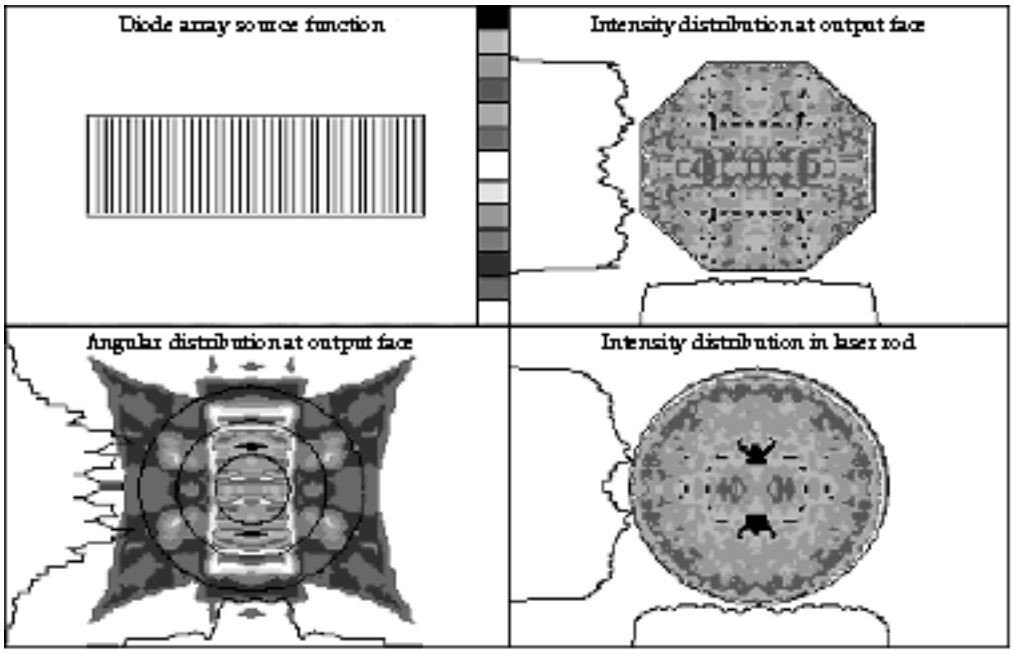

FIGURE 7. Output from our Monte Carlo ray-tracing code showing the diode-laser-array source function and the diode pump intensity at various locations in an end-pumped rod laser. (10-00-0797-1160pb01)

reflector for the laser radiation to be generated. Typically, the rods used in this approach have an optical polish along their barrel and are bathed in a coolant. Once pump light enters the laser rod, it is ducted along the length of the rod and is confined by TIR as it is absorbed. This approach allows the use of rods with light doping concentrations, compared to amounts required in a side-pumped configuration, since the available absorption paths are lengthened in the end-pumping approach. Light doping, in turn, allows the thermal load to be distributed over the entire length of the laser rod, enabling effective thermal management of the gain medium.

One problem in the practical realization of such end-pumped systems is the very high pump-power irradiances incident on the end of the laser rod. For example, in our HAP Yb:YAG DPSSL, the pump irradiance is up to 30 kW/cm^2 on the pump input end of the rod. As a result of high pump irradiances and the generated thermal power density, rod fracture at the pump input end was one of the early, but persistent, problems we encountered in developing our end-pumped system. Other practical problems are associated with cooling the end of the laser rod. Typically, the last few millimeters of a rod end cannot be effectively cooled by the water jacket around the rest of the rod because of the space required for o-ring seals. To address this thermal management problem at the pump input end of the laser rod, we use nonabsorbing or undoped rod sections that are bonded to the doped ends of the laser rod.

Figure 8 shows calculated temperature isotherms in two rods. Figure 8(a) is an ordinary, uniformly doped rod; Figure 8(b) is a composite rod with an undoped end cap. Clearly evident is an alteration of the temperature field near the end of the rod, which has two important effects. The first is related to the sensitivity of the transmission/reflection properties of dichroic coatings to temperature. In the composite rod, the coating temperature is nearly spatially uniform and very near the coolant temperature. The second benefit is associated with surface thermal stresses. The presence of temperature gradients in the rod leads to thermally induced stresses. Generally, the stresses are tensile on the rod surfaces and compressive inside the rod. Tensile stresses on the rod surfaces, where defects may be present, can lead to fracture of the laser rod. The end cap in the composite rod reduces temperature gradients near the rod end faces, thereby reducing tensile stresses and the potential for thermal fracture from face defects. In practice, we have found that such composite laser rods fabricated using a diffusion-bonding technology are extremely beneficial at enhancing the performance of our laser systems.[11] In fact, we now routinely run our systems at average powers that would not be possible without undoped end caps because of rod fracture.

Tm^{3+}:YAG HAP DPSSL

The 2-μm radiation produced by the $^3F_4$–$^3H_6$ transition of Tm^{3+} has many practical applications in medical, commercial, and military technologies. The strong absorption of radiation at this wavelength by water and human tissues is attractive for laser surgery, and the low atmospheric absorption and eye-safe properties make this system useful for materials processing, range finding, remote sensing, and other applications. In addition, 2-μm lasers are useful for pumping mid-infrared optical parametric oscillator materials, for which 1-μm radiation cannot be used. Such applications, together with the potential for efficiency, compactness, and ruggedness, have driven our interest in and the development of a HAP DPSSL Tm:YAG system.[12–18]

Because of the quasi-three-level laser properties of Tm^{3+}, intense pump sources are required for efficient operation. A major advantage of 2-μm Tm lasers is the ability to use AlGaAs diodes operating around 0.8 μm as the pump source while maintaining high efficiency and low thermal loading. This is because Tm^{3+} exhibits a beneficial two-for-one cross-relaxation process at high doping levels. The cross-relaxation process can lead to efficient laser operation, as demonstrated by measured slope efficiencies up to 59%, considerably larger than the 39% maximum expected from the quantum defect alone.[19]

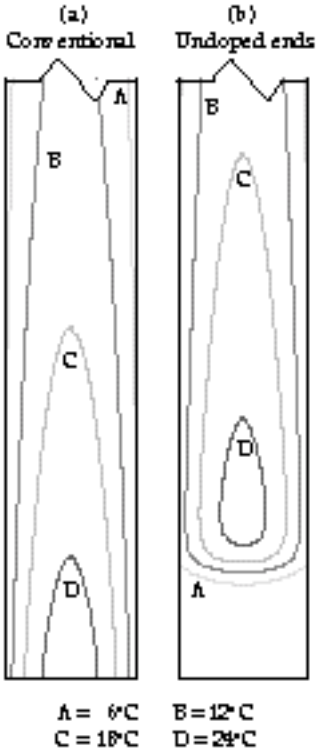

FIGURE 8. Modeled temperature profiles of a laser rod (a) with conventional, uniform doping and (b) with an undoped end cap. (70-00-0896-1881pb01)

Although the two-for-one pumping efficiency requires high doping levels, lower Tm^{3+} concentrations can be beneficial in distributing the thermal load over a longer length of the rod (for end-pumping as used here), and for reducing ground-state reabsorption losses at the laser wavelength. Therefore, a good laser design must integrate several factors, including sufficiently high dopant concentration, to obtain the best overall laser performance. Our Tm:YAG laser has generated 115 W of continuous-wave (CW) output power at 2.01 μm (multimode).[20] To our knowledge, this is the highest CW power operation achieved to date with a diode-pumped, 2-μm-wavelength laser.

Figure 9 shows the relevant components of the end-pumping technology. The pump source consists of a 2.5-cm-high, 23-module stack of microlens-conditioned, 1-cm, laser diode bars mounted on silicon microchannel coolers and producing up to 460 W of CW power reliably. The measured combined efficiency of the microlenses and lens duct is 78%, resulting in powers of up to 360 W delivered to the laser rod. The lens duct tapers to an octagonal end face to match the laser rod, with a delivered power density of more than 5 kW/cm^2.

The 3-mm-diameter by 55-mm-long laser rod has a polished barrel finish over its length, allowing pump light to be efficiently directed down the length of the rod while being confined by TIR. To decrease thermal stresses at the rod ends, 5-mm-long undoped YAG end caps are diffusion bonded to each end of the central, 45-mm-long, Tm-doped section. The pump end of the rod is coated to obtain high reflectivity at 2.01 μm (the laser wavelength) and high transmission at 0.8 μm (the pump wavelength) over wide angles. The output end of the rod has a coating that has high transmission at 2.01 μm and is a high reflector at 0.8 μm, allowing the pump light to be effectively double-passed up and down the laser rod.

For the end-pumping geometry used here, thermal management issues must be balanced with Tm concentration requirements for efficient cross relaxation. The cross-relaxation process between Tm^{3+} ions, where an ion excited to the $^3H_4$ pump level results in two ions excited to the $^3F_4$ upper laser level, requires high Tm doping levels with typical laser designs using concentrations on the order of a few percent. To incorporate the high doping levels needed for efficient cross relaxation, we use so-called "wing pumping" at 805 nm rather than the peak $^3H_6$–$^3H_4$ absorption feature at 785 nm. This distributes the pump light absorption over a longer rod length, improving pump and thermal dissipation uniformity. A further advantage of the 805-nm pump wavelength is reduced Al concentration in the AlGaAs diodes, increasing output performance and reliability relative to the 785-nm diodes that would be used to pump the Tm^{3+} at the peak of its $^3H_6$–$^3H_4$ absorption.

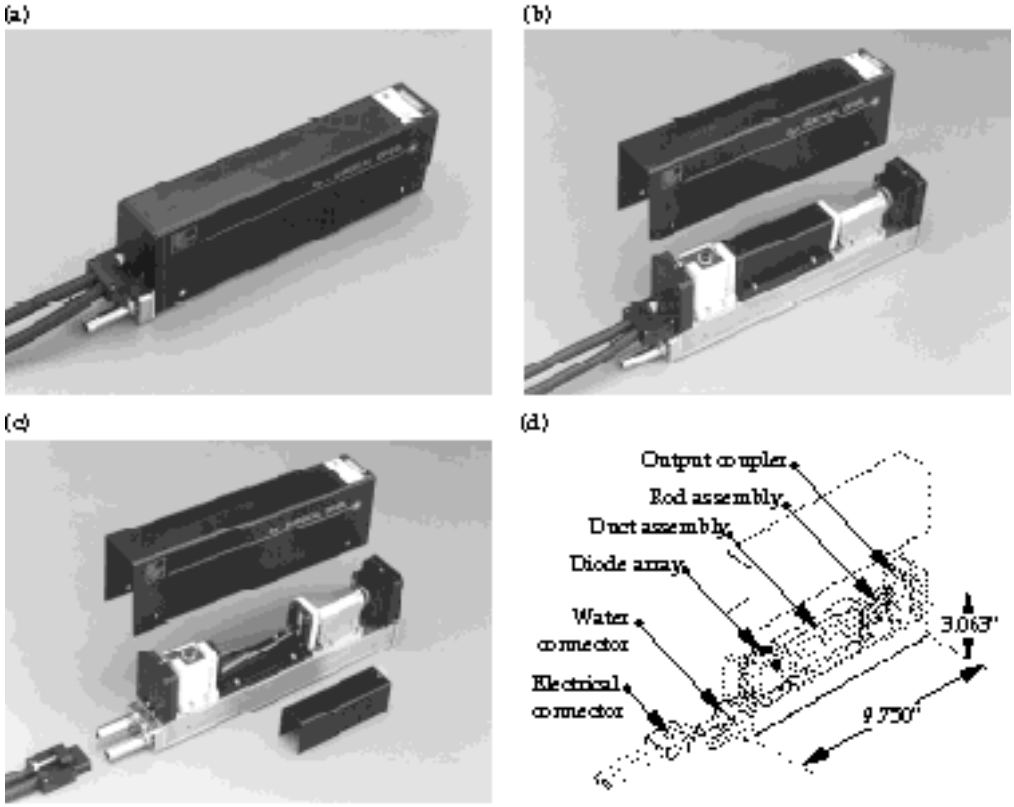

FIGURE 9. Photographs and sketch of 2-μm Tm:YAG laser. (70-15-0294-0287pb04)

Figure 10 shows laser power vs diode pump power delivered to the Tm:YAG laser rod for 2% and 4% doping levels, obtained with a 95.2%-reflective, 50-cm concave output coupler and a cavity length of 6 cm. The output power for the 2% Tm rod increases up to 115 W for a delivered pump power of 360 W; whereas the 4% rod shows a significantly higher threshold and a maximum power of 74 W. Laser power measurements were also obtained with flat output couplers of various reflectivities, although the maximum power observed (again with the 2% rod) was approximately 10% less than with the concave reflector. The slope efficiencies in Figure 10 are similar for the two doping levels, with the 2% rod yielding an intrinsic slope efficiency of 40% relative to pump power delivered to the rod. A small reduction in slope efficiency occurs at the highest powers, possibly due to thermal effects.

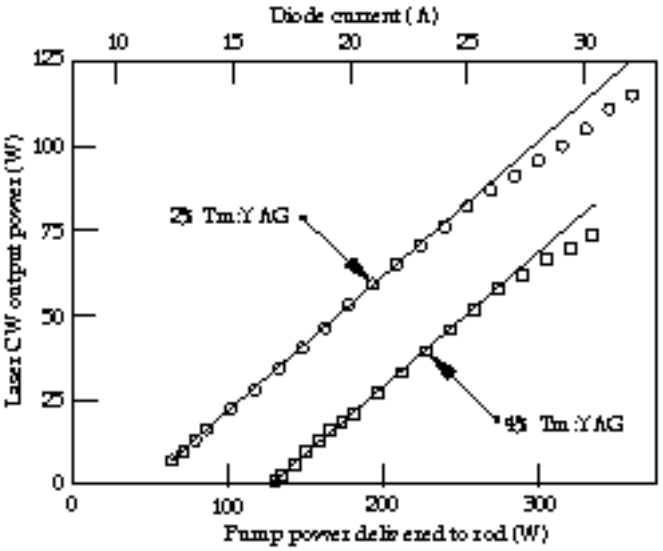

FIGURE 10. Tm:YAG laser CWoutput power at 2 μm vs pump power delivered to the laser rod for 2% and 4% Tm-doped rods. The output coupler is concave with a 50-cm radius of curvature and a reflectivity at 2.01 μm of 95.2%. (10-00-0797-1158pb01)

We can compare measured laser performance with that predicted by a quasi-three-level laser model developed by our group.[21] By measuring laser power as a function of input power for various output coupler reflectivities, we can determine values for T_{cav}, the one-way cavity transmission, η_{mode}, the mode-fill efficiency, and η_{QY}, the quantum yield, which are difficult to obtain from more direct measurements. Figure 11 shows a set of measurements for the 2% Tm rod, with laser thresholds and slope efficiencies plotted vs output coupler reflectivity. The measurements are compared to a simultaneous least-squares fit using the model to determine $\eta_{mode} = 0.92$, $\eta_{QY} = 1.88$ and $T_{cav} = 0.997$. Each value is near the maximum expected, consistent with the high power and efficient operation achieved. Note that η_{QY} is still quite high, although the Tm doping level is only 2%, whereas the high value of η_{mode} reflects the multiple transverse laser modes that nearly fill the rod cross section.

From Figure 11, we see that the model generally overestimates the threshold power. The overestimation is possibly due to nonuniform pump light across the rod cross section because threshold could be reached for some fraction of the rod before the entire rod had sufficient gain to overcome losses. The slope efficiencies are relative to the pump power delivered to the rod, although the fraction of pump energy absorbed, f_{abs}, is estimated to be only 77% for the 2% Tm rod. Therefore, the slope efficiency relative to absorbed pump power is 52% for the 2% Tm data shown in Figure 11, which compares favorably with values reported for lower-average-power systems.[16]

Figure 12 shows the M^2 beam-quality factor against pump power, which is proportional to the square root of the delivered pump power. This observation has been analyzed in terms of a gradient lens model of

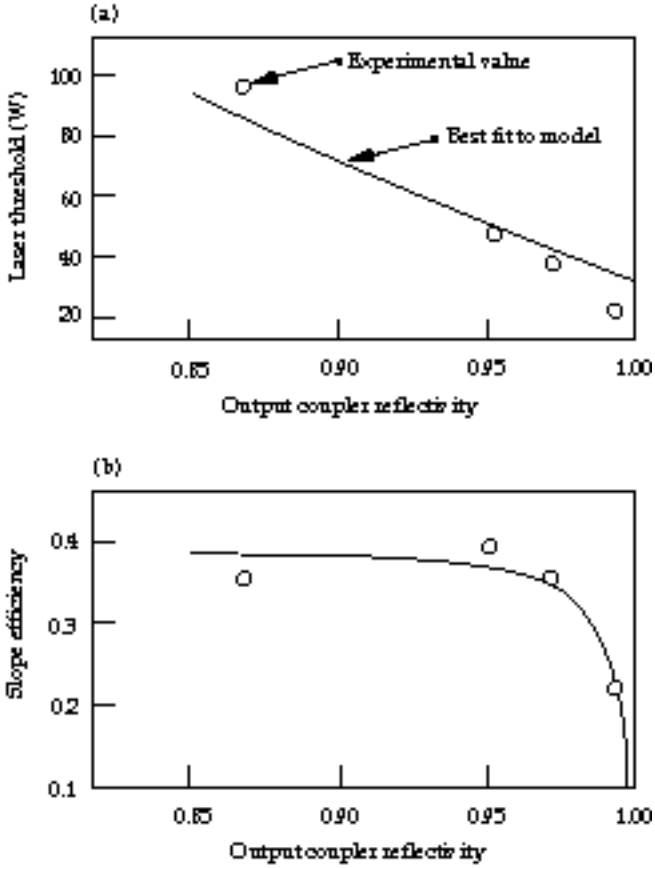

FIGURE 11. Comparison between best-fit model predictions and measured (a) laser threshold and (b) slope efficiency vs output coupler reflectivity for the 2% Tm-doped rod. (10-00-0797-1159pb01)

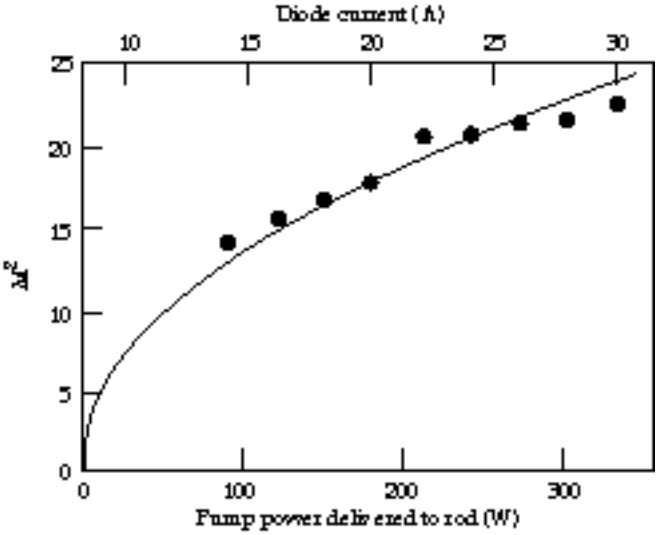

FIGURE 12. Plot of M^2 vs laser diode pump power. (10-00-0797-1157pb01)

thermal focusing in the laser rod, and the expectation that the fundamental beam mode scales as $P^{1/4}$. The model appears to give the correct scaling behavior; however, the measured scaling factor based on the model is 3.1 times greater than the calculated value. Although the measured beam quality is far from diffraction-limited, there are a broad range of applications for which M^2 values of 20 and less are useful.

Yb^{3+}:YAG HAP DPSSL

The Yb^{3+}:YAG system we are presently developing is particularly attractive to many applications now using Nd^{3+}:YAG because the Yb^{3+} ion only generates about one-third the heat of an excited Nd^{3+} ion. The lower heat generation is due predominantly to the lower Stokes shift, or quantum defect, between pump and laser photon energy of the Yb^{3+} ion compared to the Nd^{3+} ion. Because system efficiency of a Yb^{3+}-based system is expected to be approximately the same as that of a Nd^{3+}-based system, the thermal management problems in the Yb^{3+} system should be substantially reduced from those in Nd^{3+} systems of comparable power. The reduced thermal heat load of Yb^{3+} should ultimately allow HAP DPSSL systems with better beam quality and higher average power than are now possible with Nd^{3+}.

In addition to these thermal management issues, the broad pump line at 940 nm makes the Yb:YAG system highly suitable for diode pumping using InGaAs diodes, which are more robust than the AlGaAs diodes used to excite Nd:YAG at approximately 808 nm. Recent results from lifetime tests on LLNL-fabricated 940-nm diode packages have shown projected lifetimes of more than 10,000 hours (with 30% degradation) when operated at 30 W/cm (Ref. 22). Another advantage of Yb:YAG is that the 940-nm absorption feature is approximately 10 times broader than the 808-nm absorption feature in Nd:YAG; therefore, the Yb:YAG system is less sensitive to diode wavelength specifications. These advantages of Yb over Nd-based systems, together with a broad spectrum of laser applications, have prompted the Laser Programs' interest in developing a Yb^{3+}:YAG HAP DPSSL.[23]

Figure 3 shows our end-pumped Yb:YAG laser system, which is similar to the Tm:YAG system previously described. The pump source consists of a 44-bar stack of 1.5-cm-long InGaAs laser diode bars packaged on microchannel coolers. As in the Tm:YAG laser, the diode light is first conditioned by a shaped cylindrical microlens directly mounted on each diode package, and then delivered to the composite Yb:YAG rod via a lens duct. The Yb:YAG composite rod is coated at the pump end of the rod with a dichroic coating having high reflectance at 1030 nm and high transmission at 940 nm, thus allowing one end of the rod to perform as a flat, high reflector for the laser cavity. A simple, broadband antireflection coating was placed on the opposite or output end of the rod.

We have demonstrated the Yb:YAG laser in both CW and Q-switched operation. The doping concentration for our CW experiments was 0.44%, and the rod diameter was 2 mm with an overall composite length of 60 mm. The laser crystal was housed in a simple aluminum cooling jacket designed to flow coolant along the barrel of the rod. The rod temperature was maintained near 0°C by using a mixture of water and propanol. Approximately 63% of the pump light was transmitted through the microlenses and lens duct into the laser rod. Of the light transmitted into the rod, approximately 80% was absorbed within the laser rod. Figure 13 shows the Yb:YAG CW output power against the power generated at the laser diode array. The maximum CW output power of 434 W more than doubles the average power generated in this type of system by any other research group at this time. Based on our quasi-three-level models, we anticipate generating more than 500 W in the near future with improved optical coatings on the laser rods.

Our Yb:YAG system distinguishes itself from comparable average-power Nd:YAG systems in the output beam quality that is generated. Typically, Nd:YAG rod laser systems in this average power class produce output beams with M^2 values of 30 or larger. Using a conventional stable resonator, the measured M^2 of the Yb:YAG system was 6.5 at an output power level of 190 W. The predominant reasons for better beam quality with the Yb:YAG system are the lower thermal power generated by Yb compared to Nd, and the much smaller rod diameter of the Yb:YAG system relative to a Nd:YAG system. The smaller rod diameter

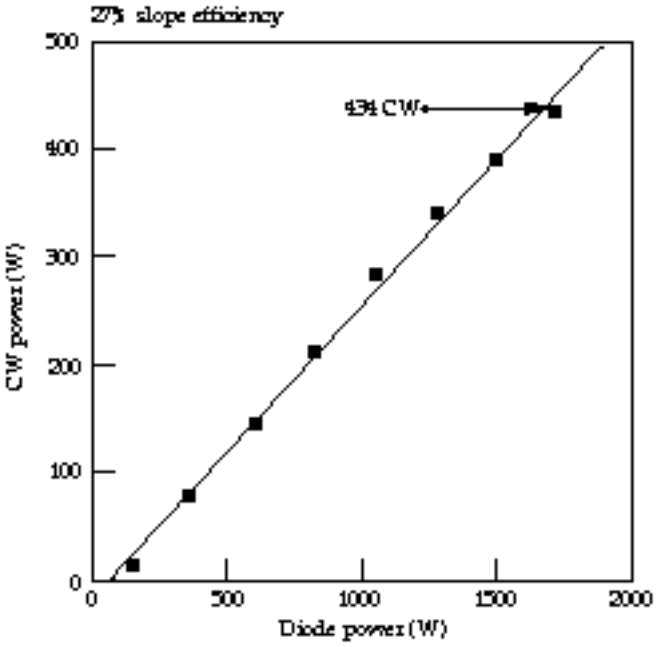

FIGURE 13. Yb:YAG laser output power at 1 μm vs pump power delivered to the laser rod. (10-00-0797-1156pb01)

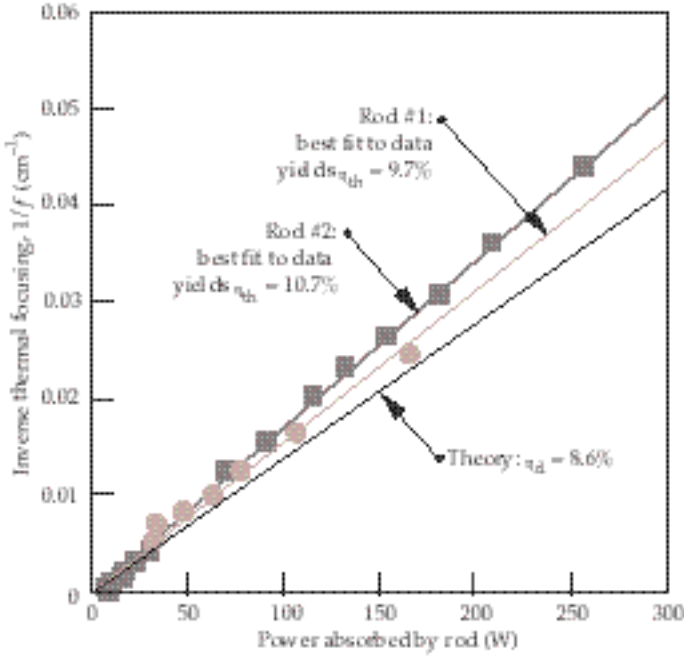

FIGURE 14. Inverse thermal focusing in Yb:YAG laser rod as a function of absorbed pump power. (10-00-0797-1155pb01)

essentially limits the number of transverse modes the Yb:YAG laser can support.

To document the thermal-generation properties of the Yb:YAG system, we measured thermal lensing and stress-induced birefringence. Measured thermal-generation rates are in close agreement with values expected using the quantum defect value of 8.6% for Yb:YAG. A probe beam at 632 nm was used to measure the thermal lensing of the laser rod. Two different rods were used in the measurements shown in Figure 14. The best fit to the data yielded an average thermal efficiency factor of 10.2%, where thermal efficiency η_{th} is defined as the percent of pump power dissipated as heat into the rod. Measurements of stress-induced birefringence were made using a 1.03-μm probe beam. The best fit to the data yielded a thermal efficiency factor of 8.74%. The average result from both types of measurements gives $\eta_{th} = 9.5\%$.

We also generated Q-switched pulses at high repetition rate using an acousto-optic Q-switch. In this work, the laser rod was pumped continuously, as in the CW operation of the system, and the acousto-optic Q-switch was gated off at various repetition rates between 5 and 20 kHz. To date, our best result is an average output power of 285 W at 10 kHz. Based on a Q-switched, quasi-three-level model we have developed, we expect to achieve more than 300 W of Q-switched power with better-performing optical coatings on the laser rod.[24] Under such conditions, the resulting Q-switched pulse width was 26 ns. This Yb:YAG Q-switched pulse width is substantially shorter than values demonstrated with comparable Nd systems and is presently being used to investigate the feasibility of high-average-power, external-cavity harmonic generation.

Summary

We are continuing to develop high-average-power, diode-array, end-pumping technology in an effort to move HAP DPSSL systems beyond the Nd^{3+} ion. To date, most of our work has concentrated on two systems that are perceived to have near-term applications. The first system is based on the Tm^{3+} ion and generates output radiation at 2 μm. To date, we have demonstrated more than 100 W of CW output from a compact, efficient, and reliable diode end-pumped Tm:YAG laser system. Using a quasi-three-level laser model, we find that the cross relaxation in Tm:YAG can be quite efficient at a doping level of 2%. The use of this relatively low doping level, while maintaining efficient cross relaxation, is beneficial to thermal management issues necessary for scaling to high average powers. The second system is based on the Yb^{3+} ion and generates output radiation at 1 μm. To date, we have demonstrated up to 434 W of CW power from an end-pumped Yb:YAG laser system. In addition, at a 10-kHz repetition rate, we have produced up to 285 W of Q-switched power at a 26-ns pulse length. The short pulse widths and better beam quality that can be generated with the Yb:YAG system, relative to comparable average-power Nd:YAG systems, highlight the unique capabilities of the Yb:YAG system.

Acknowledgments

We wish to acknowledge many useful conversations with Steve Payne, Bill Krupke, Rich Solarz, Mark Emanuel, Jay Skidmore, Ralph Page, John Crane, Isaac Bass, Gaylon Erbert, Chris Marshall, and Howard Powell, all of LLNL, during the course of this work. We also acknowledge the expert laser technical assistance of Scott Mitchell and Joel Speth. In addition, we thank Steve Mills, Dennis Maderas, John Lang, Barry Freitas, Chuck Petty, Vic Sperry, Evert Utterback, Kathy Reinhardt, and Larain Dimercurio, all of LLNL, in carrying out various portions of the work reported. We also thank Dr. Helmuth Meissner of ONYX Optics for fabricating the composite laser rods with diffusion-bonded end caps, Ralph Hucheson of Scientific Materials for growing the YAG crystals used in our lasers, and Karl George of Quality Thin Films for supplying the optical coatings used on our laser rods.

Notes and References

1. N. G. Basov, O. N. Krokhin, and M. Popov, "Production of Negative Temperature States in P–N Junctions of Degenerate Semiconductors," *J.E.T.P.* **40**, 1320 (1961).
2. L. J. Mawst et al., "8-W Continuous Wave Front-Facet Power from Broad-Waveguide Al-Free 980-nm Diode Lasers," *Appl. Phys. Lett.* **69**, 132 (1996).
3. W. Koechner, *Solid-State Laser Crystals* (Springer-Verlag, Berlin, 1976).
4. R. Beach et al., "Scaleable Diode-End-Pumping Technology Applied to a 100-mJ Q-Switched Nd^{3+}:YLF Laser Oscillator," *Opt. Lett.* **18**, 1326–1328 (1993).
5. R. Beach et al., "Modular Microchannel Cooled Heatsinks for High Average Power Laser Diode Arrays," *IEEE J. Quant. Elect.* **28**, 966–976 (1992).
6. J. Snyder, P. Reichert, and T. Baer, "Fast Diffraction-Limited Cylindrical Microlenses," *Appl. Opt.* **30**, 2743–2747 (1991).
7. R. Beach et al. "Applications of Microlens-Conditioned Laser Diode Arrays," *SPIE* **2383**, 283–297 (1995).
8. R. Beach, "Theory and Optimization of Lens Ducts," *Appl. Opt.* **35**, 2005–2015, (1996).
9. W. T. Welford and R. Winston, *High Collection Nonimaging Optics* (Academic Press, New York, 1989).
10. J. K. Crane et al., *Description and Performance of the Preamplifier for the National Ignition Facility (NIF) Laser System*, UCRL-JC-124517, Lawrence Livermore National Laboratory, Livermore, CA (preprint).
11. ONYX Optics, 6546 Sierra Lane, Dublin, CA 94568, Tel: 510-833-1969.
12. G. J. Kintz, R. Allen, and L. Esterowitz, *Digest of Conference on Lasers and Electro-Optics*, paper FB2 (Optical Society of America, Washington, D.C., 1988).
13. P. Suni and S. Henderson, *Opt. Lett.* **16**, 817–819 (1991).
14. T. S. Kubo and T. J. Kane, *IEEE J. Quant. Elec.* **28**, 1033–1040 (1992).
15. D. C. Shannon, D. L. Vecht, S. Re, J. Alonis, and R. W. Wallace, *Proc. SPIE* **1865**, 164–173 (1993).
16. G. Rustad, H. Hovland, and K. Stenersen, *OSA Proceedings on Advanced Solid State Lasers*, S. Payne and C. R. Pollock, Eds., *Opt. Soc. Amer.* **15**, 315–318 (1996).
17. S. R. Bowman et al., *OSA Proceedings on Advanced Solid State Lasers*, A. Pinto and T. Y. Fan, Eds., *Opt. Soc. Amer.* **15** (1993).
18. I. F. Elder and M. J. P. Payne, *OSA Proceedings on Advanced Solid State Lasers*, S. A. Payne and C. R. Pollock, Eds., *Opt. Soc. Amer.* **15**, 319–325 (1996).
19. R. C. Stoneman and L. Esterowitz, *Opt. Lett.* **15**, 486–488 (1990).
20. E. C. Honea et al., *High Average Power Tm:YAG Diode-Pumped Solid-State Laser*, UCRL-JC-125109, Lawrence Livermore National Laboratory, Livermore, CA (preprint).
21. R. Beach, "CW Theory of Quasi-Three-Level End-Pumped Laser Oscillators," *Optics Comm.* **123**, 385–393 (1995).
22. M. A. Emanuel, J. A. Skidmore, and R. J. Beach, "High-Power Laser Diodes at Various Wavelengths," *SPIE Photonics West 1997 Proc.*, paper 3001-1 (1997).
23. H. Bruesselbach and D. Sumida, "69-W-Average-Power Yb:YAG Laser," *Opt. Lett.* **21**, 480–482 (1996).
24. R. Beach, "Optimization of Quasi-Three-Level End-Pumped Q-Switched Lasers," *IEEE J. Quant. Elec.* **31**(9), 1606–1613 (1995).